Rotation and Deformation of a Finitely Extendable Flexible Polymer Molecule in a Steady Shear Flow

Carsten Aust,[†] Siegfried Hess,[†] and Martin Kröger*[,†,‡]

Institut für Theoretische Physik, Technische Universität Berlin, Hardenbergstrasse 36, D-10623 Berlin, Germany; and Polymer Physics, Materials Sciences, ETH Zürich, CH-8092 Zürich, Switzerland

Received May 8, 2002; Revised Manuscript Received August 8, 2002

ABSTRACT: In this article, we establish the validity of a relation between the true angular velocity and gyration tensor for a dilute polymer solution in the case of a steady shear flow by means of nonequilibrium molecular dynamics computer simulation. The microscopic model for a polymer molecule immersed in a solution composed of monomers incorporates the effects of hydrodynamic interaction through the presence of explicit solvent monomers and the effect of finite stretchability of chains. In the strong flow regime, we observe regular and irregular dynamical behavior which is inherently connected with the nonlinearities in the equations of motion which come along with finite extendability of polymer chains. The microscopic dynamics underlying the simple relationship, and in particular the time series, the correlated rotation and deformation behavior, and cross-correlations between several structural quantities are investigated in detail. The results allow for a test of more efficient implementations, which aim to describe polymer dynamics considering hydrodynamic interactions by using ad hoc Langevin equations for the conformational variables.

I. Introduction

The shear-induced rotation and the conformational changes of flexible chain molecules subjected to a simple shear flow in a dilute solution are closely coupled. The same applies to the partial orientation of molecules seen in long time averages. Macroscopic, non-Newtonian rheological properties of polymer solutions, such as flow-dependent viscosities and normal stresses, result from microscopic stresses that arise when polymeric molecules undergo conformational changes and affect the solvent motion. Thus, much effort has been directed at predicting the dynamics of polymers in shear flows.[1] However, it has been difficult to rigorously test underlying predictions on the molecular scale. Experimental efforts have mainly focused on measuring bulk rheological properties or on measuring the scattering of light or neutrons by polymer solutions,[2] and computer simulation studies often focused on macroscopic quantities such as the time averaged end-to-end distance[3−5] rather than correlating conformation with angular velocity.

So far, information on the ensemble-averaged angular velocity can only be inferred from the behavior of components of the gyration tensor averaged over many molecules.[6] This estimate for the angular velocity relies on a theoretical relation[7] based on approximations. The limits of applicability have yet to be tested by experiments as reported in ref 8, where the possibility to observe directly the effect of a shear flow on the shape of an individual molecule was demonstrated. Both the conformational changes as characterized by the gyration tensor, end-to-end distances, and further ensemble-averaged quantities can and have been extracted for a long time from nonequilibrium molecular dynamics (NEMD)[9,10] and nonequilibrium Brownian dynamics[3,4] computer simulations. Correlations, on the other hand, such as those between deformation and rotation of molecules, received a minor attention in simulations and were often discussed qualitatively and by showing snapshots but were not fully analyzed in a more quantitative fashion. This fact alone gives evidence for a rather complicated motion of finitely extendable polymers subjected to shear flow, while the conformational behavior in extensional flows is comparatively well understood.[11] Because the hydrodynamic interactions are reduced by stretching, a solute polymer coil should unwind abruptly when a certain critical value of the velocity gradient is reached. In ref 12, the effect of "flexibility" (through a broken-rod model) of molecules on their rotation behavior under shear had been investigated. Even though this model was devoted to study polymers in the nematic phase, flexibility was surprisingly not preventing a complex rotational dynamics known for rodlike liquid crystals, see, e.g., refs 13−15. It is important to notice that complex dynamics is inherently connected with the nonlinearities in the equations of motion which come along with finite extendability (anharmonic bond potentials) or stiffness of polymer chains.

In this article, we present further results calculated in NEMD simulations as described in ref 10. The system studied consists of single finitely extendable chains of different lengths, immersed in a solution composed of the monomers whose microscopic dynamics is also dealt with. Here, NEMD results are presented, which allow one to test a relation between the angular velocity obtained from the angular momentum divided by the relevant moment of inertia and a ratio of components of the gyration tensor. Furthermore, the time behavior of various structural properties is analyzed, and time correlation functions and cross-correlations are presented. To motivate the following analysis, we begin with a simple derivation of an approximate relationship, which connects angular velocity with components of the tensor of gyration for a stiff particle of arbitrary shape.

[†] Technische Universität Berlin.
[‡] ETH Zürich.

10.1021/ma020710k CCC: $22.00
Published on Web 09/28/2002

II. Angular Velocity and Configurational Properties

A. Derivation of a Relation between Angular Velocity and the Molecular Shape. A stiff particle immersed in a fluid undergoing a shear flow picks up an angular velocity equal to the local vorticity which, in turn, is half of the rotation (curl) $\nabla \times \mathbf{v}$ of the velocity field $\mathbf{v}$. Flexible chain molecules are deformed by the shear flow, and their average angular velocities, given by the ratios of their angular momenta and their moments of inertia, decrease with increasing shear rates. This was first conjectured on the basis of a relation between this angular velocity and a ratio of components of the gyration tensor, discussed within the framework of a theory associated with the key word "internal viscosity".[7] Here, a simpler derivation of such a relation is given, in the spirit of the ideas put forward by Debye.[16] Consider a chain molecule composed of N beads with mass m located at positions $\mathbf{r}^i$ with $i = 1, 2, ..., N$. Each bead is assumed to obey an equation of motion of the form

$$m \frac{\mathrm{d}^2\mathbf{r}^i}{\mathrm{d}t^2} = \mathbf{F}^i - m\zeta\left(\frac{\mathrm{d}\mathbf{r}^i}{\mathrm{d}t} - \boldsymbol{v}(\mathbf{r}^i)\right) \tag{1}$$

The term involving the friction coefficient ζ is the friction force the bead experiences when it moves relative to the flow velocity $\mathbf{v}$ the solution would have in the absence of the polymer chain. The quantity $\mathbf{F}^i$ stands for all other forces acting on the bead "i". The time change of the total angular momentum $\mathbf{L} = m \sum_i \mathbf{r}^i \times \mathrm{d}\mathbf{r}^i/\mathrm{d}t$ is given by

$$\frac{\mathrm{d}\mathbf{L}}{\mathrm{d}t} = \sum_i \mathbf{r}^i \times \mathbf{F}^i - \zeta(\mathbf{L} - m \sum_i \mathbf{r}^i \times \mathbf{v}(\mathbf{r}^i)) \tag{2}$$

The first term on the rhs corresponding to a torque vanishes for central forces. Also the time change of the angular momentum is assumed to vanish when averaged over long times. Then (2) leads to

$$\langle \boldsymbol{L} \rangle = m \langle \sum_i \mathbf{r}^i \times \mathbf{v}(\mathbf{r}^i) \rangle \tag{3}$$

The angular bracket indicates the time average. The friction coefficient ζ disappeared from this relation since it was assumed to be constant.

An angular velocity $\bar{\omega}$ is defined as the ratio of $\langle \mathbf{L} \rangle$ and of the relevant component of the (time averaged) moment of inertia tensor. To be more specific, a plane Couette geometry is considered with the flow in the x-direction and the gradient of the velocity in the y-direction; viz., $v_x = \dot{\gamma} y$, $v_y = v_z = 0$, where $\dot{\gamma} = \partial v_x/\partial y$ is the (constant) shear rate. Then (3) is equivalent to

$$\langle L_z \rangle \stackrel{?}{=} -\dot{\gamma} m \langle G_{yy} \rangle \tag{4}$$

The question mark intends to remember, that this relationship is based on assumptions. Here G_{yy} is the yy-component of the gyration tensor

$$G_{\mu\nu} = \sum_i \mathrm{r}_\mu{}^i \mathrm{r}_\nu{}^i \tag{5}$$

Greek subscripts indicate Cartesian components. It is understood that the center of mass of the polymer chain corresponds to $\mathbf{r} = 0$, i.e., one has $\sum_i \mathbf{r}^i = 0$. For the present geometry, the relevant moment of inertia is $m(G_{xx} + G_{yy})$. Thus, the expression for the angular velocity, inferred from the average angular momentum is

$$\bar{\omega} = \frac{\langle L_z \rangle}{m(\langle G_{xx} \rangle + \langle G_{yy} \rangle)} \tag{6}$$

Relation 4 becomes

$$\bar{\omega} \stackrel{?}{=} \bar{\omega}_G \tag{7}$$

with the expression $\bar{\omega}_G$ based on the geometry of the polymer coil given by

$$\bar{\omega}_G = -\dot{\gamma} \frac{\langle G_{yy} \rangle}{\langle G_{xx} \rangle + \langle G_{yy} \rangle} = -\frac{\dot{\gamma}}{2}\left(1 - \frac{\langle G_{xx} \rangle - \langle G_{yy} \rangle}{\langle G_{xx} \rangle + \langle G_{yy} \rangle}\right) \tag{8}$$

In the equilibrium state, i.e., $\dot{\gamma} = 0$, the coil is spherical on average and one has $\bar{\omega}_G = -\dot{\gamma}/2$. The same applies for small shear rates. At intermediate and at high shear rates, the polymer molecule is substantially deformed such that $G_{xx} > G_{yy}$, on average. This implies that the dimensionless ratio $\bar{\Omega}_G \equiv -\bar{\omega}_G/\dot{\gamma}$ becomes significantly smaller than $^1/_2$ which is its small shear rate-limiting value. A relation of the form shown in (7) between the rotational angular velocity $\bar{\omega}$ and the quantity $\bar{\omega}_G$ associated with the deformation of the chain molecule was first proposed by R. Cerf.[7] Nonequilibrium molecular dynamics (NEMD) computer simulations allow for a test of this and an analogous relation involving averages of ratios rather than ratios of averages, viz.

$$\langle \omega \rangle \stackrel{?}{=} \langle \omega_G \rangle \tag{9}$$

with

$$\omega = \frac{L_z}{m(G_{xx} + G_{yy})}, \quad \omega_G = -\dot{\gamma} \frac{G_{yy}}{(G_{xx} + G_{yy})} \tag{10}$$

For convenience, we will discuss results in terms of the four corresponding dimensionless angular velocities (capital ω); i.e., the rewritten hypothetical eqs 7 and 9 read

$$-\frac{\bar{\omega}}{\dot{\gamma}} \equiv \bar{\Omega} \stackrel{?}{=} \bar{\Omega}_G \equiv -\frac{\bar{\omega}_G}{\dot{\gamma}} \tag{11}$$

$$-\frac{\langle \omega \rangle}{\dot{\gamma}} \equiv \langle \Omega \rangle \stackrel{?}{=} \langle \Omega_G \rangle \equiv -\frac{\langle \omega_G \rangle}{\dot{\gamma}} \tag{12}$$

B. Goal. If the simple assumptions made are valid, eq 4 should hold. When the fluctuations of the moment of inertia with time are not too large $\bar{\omega} \approx \langle \omega \rangle$ as well as $\omega_G \approx \langle \omega_G \rangle$ can be expected. The result obtained in the previous paragraph (eqs 7 and 11) based on the underlying simple model, however, should not be expected to hold within a refined description for the dynamics of a polymer chain. Starting from a microscopic model which does not rely on the assumptions made, here a test is performed between the "true" angular velocities, $\langle \omega \rangle$ or $\bar{\omega}$ and their configurational counterparts $\langle \omega_G \rangle$ and $\bar{\omega}_G$.

In the NEMD simulations to be presented next, both the polymer and the solvent molecules were treated microscopically, i.e., no friction coefficient is introduced, in contradistinction to Brownian dynamics simula-

tions.[17,3] This allows us to unambiguously comment on the validity of eqs 7 and 9 or equivalently 11 and 12.

Our goal here is to determine whether eq 4 and the implied equivalence between $\bar{\omega}$ and $\bar{\omega}_G$ are approximately valid. We further aim to provide insight into the underlying microscopic dynamics. Analytically treatable models tend to predict $\bar{\omega}_G$ rather than $\bar{\omega}$, and the former is directly related to the structure factor of polymer chains in the Guinier regime.[18] The quantity $\bar{\omega}$, however, is related to the correct definition of the angular momentum, i.e., the lhs of "eq" 4, whose validity comes together with the underlying assumptions. A closely related topic concerns the prediction of the stress tensor, if angular momentum **L** is replaced by **rF** in the discussion. Simple models yield, e.g., an equation formally comparable with (4) where the stress tensor (material function) appears on the lhs, and the averaged conformational (optical) quantity on the rhs.[19,2] Such equations are known as stress−optic laws, or—more precisely—as stress−optic rules. Equation 4, which implies (7), may be considered as an angular momentum−optic rule therefore.

C. NEMD Simulation Method and Simulation Parameters. We will shortly summarize the simulation method for the microscopic model of a dilute polymer solution under good solvent conditions, although details can be found in ref 10. The system under study consists of a single linear chain of $N = 10-60$ linearly connected identical particles (beads) "confined" in a periodic simulation cell, and dissolved in a bath of explicit solvent particles (unconnected beads), such that finite-size effects can be neglected. All particles interact via the repulsive part of a radial-symmetric Lennard-Jones potential $U^{\mathrm{WCA}}(r) = 4(r^{-12} - r^{-6}) + 1$,[20] cut off at $r = 2^{1/6}$. Dimensionless units are used throughout this manuscript. Thermomechanical properties of the WCA model in both its fluid and solid states are known.[21] Simulations are performed at bead number density $\rho = 0.864$ and temperature $T = 1.2$. The connectivity between beads is ensured by adding a nonlinear (and diverging) attractive potential:[22] $U^{\mathrm{FENE}}(r) = -14 \ln(1 - (r/2)^2)$, cf.,[17,10] acting between adjacent beads along the chain's contour. The flow is imposed by applying a homogeneous shear algorithm[23] together with Lees−Edwards boundary conditions.[24] Newton's equations of motion are integrated by a velocity−Verlet algorithm with an integration time step $\Delta t = 0.005$ for shear rates $\dot{\gamma} < 0.6$ and $\Delta t = 0.003/\dot{\gamma}$ for $\dot{\gamma} \geq 0.6$. Data to be presented stems from 5×10^3 and 4×10^4 time units at high and low shear rates, respectively. The first 20% of these runs are discarded in the analysis. The temperature is kept constant (NVT ensemble) by rescaling the magnitude of the particle peculiar velocities, which corresponds to the Gaussian "least constraint" thermostat[23] for $\Delta t \ll 1$. We study the effect of shear flow and chain length N, where the shear rate $\dot{\gamma}$ is varied over a range of about four decades up to $\dot{\gamma} = 3$. Above this rate the polymer chains tend to break.

D. Test of Angular Velocity Relations. A direct verification of eq 4 is made in Figure 1, where the average angular momentum $\langle L_z \rangle$ is compared to the rhs of (4), $\langle L_G \rangle$, with $L_G \equiv -\dot{\gamma} m_G yy$. To obtain a master plot for all chain lengths, the quantities are plotted vs a reduced shear rate $\beta_{\mathrm{L}} = \tau_{\mathrm{L}}\dot{\gamma}$ with the relaxation time $\tau_{\mathrm{L}} = 15$, 49, 97, and 320 for chains with $N = 10$, 20, 30, and 60 beads, respectively. Here, and also for the next figures, Figures 2 and 3, curves are fit functions (with two parameters) of a form used previously for rheological data,[25] viz. fit$(\dot{\gamma}) = 0.5(1 + (\dot{\gamma}\tau)^{\kappa})^{\mu/\kappa}$, where κ is adjusted to fit the width of the transition region around $\beta = \dot{\gamma}\tau = 1$ (here $\kappa = 1.2$ is an appropriate value used throughout the manuscript) with a dimensionless shear rate β, and μ is the relevant exponent in the high shear rate power law regime. The two angular momenta shown in Figure 1 decrease with increasing shear rate in a qualitatively similar way, with a power law $\mu = -0.45$. The reduced shear rate β_{L} was extracted here for the angular momentum from Figure 1. For Figures 2 and 3, where angular velocities are shown, slightly different relaxation times are used to produce the master plots. Specifically, for the Ω-quantities we obtain $\beta_\omega = \tau_\omega\dot{\gamma}$ with the relaxation time $\tau_\omega = 7$, 35, 90, and 440 for chains with $N = 10$, 20, 30, and 60 beads, respectively. The latter reduced rates are identical in the following to allow for a simple comparison between data for comparable quantities.

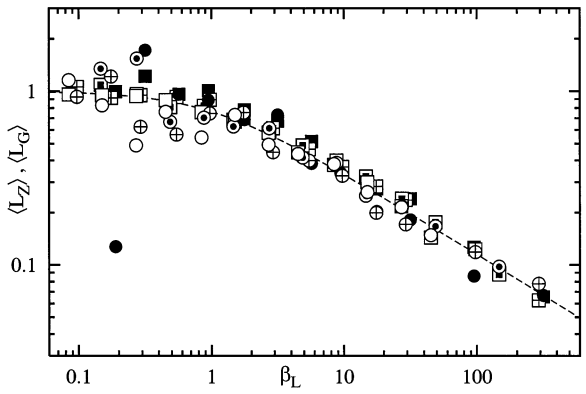

Figure 1. Simulation results for the left and right-hand sides of eq 4, i.e., average angular momentum $\langle L_z \rangle$ (squares) and $\langle L_G \rangle \equiv -\dot{\gamma} m \langle G_{yy} \rangle$ (circles). To obtain a master plot, both quantities are plotted vs a reduced shear rate $\beta_{\mathrm{L}} \equiv \tau_{\mathrm{L}}\dot{\gamma}$ with relaxation times $\tau_{\mathrm{L}} \approx 0.3\dot{\gamma}N^{1.7}$ (precise values are given in the text) which scale with chain length N. Symbols correspond to data for $N = 10$ (open), $N = 20$ (pointed), $N = 30$ (crossed), and $N = 60$ (filled).

All results shown in Figures 2 and 3 obtained for reduced angular velocities Ω at small shear rates agree with the limiting value $^1/_2$, which is indicated by the dashed line. Relation 9, which relates averages of ratios rather than ratios of averages and which can be considered as an additional measure provided by simulation, is tested in Figure 2. Both quantities $\langle \Omega \rangle$, $\langle \Omega_G \rangle$ are strongly related, fall on mostly the same curve, and possess the same power law exponent, $\mu \approx -0.75$.

In view of these findings, we finally wish to compare one of the quantities $\langle \Omega \rangle$, $\langle \Omega_G \rangle$ shown in Figure 2 with one of those, $\bar{\Omega}$, $\bar{\Omega}_G$, related to the angular momentum shown in Figure 1. In Figure 3 we therefore plot together $\langle \Omega \rangle$ and $\bar{\Omega}_G$ vs reduced shear rate. For the variable $\bar{\Omega}_G$, the decrease with shear rate is somewhat faster ($\mu = -0.85$) than the one for $\langle \Omega \rangle$, which quantifies the difference between the quantities given in (9) and (7) at intermediate and high shear rates.

To summarize, we have shown in this introductionary section, that the angular momentum−optic rule in its two identical representations, eqs 1 and 7, is validated from computer simulation, i.e.,

$$\bar{\omega} \approx \bar{\omega}_G \tag{13}$$

and that the quantities G_{xx}, G_{yy}, L_z perform correlated motions, since $|\langle \omega \rangle| > |\bar{\omega}|$, and $|\langle \omega_G \rangle| > |-\omega_G|$. We further

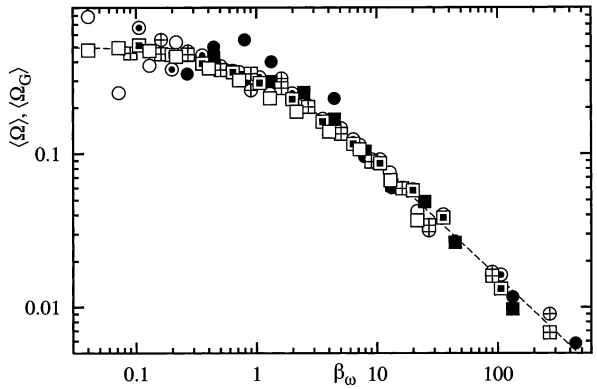

Figure 2. Simulation results for the left and right-hand sides of eq 9 (or alternatively eq 12), i.e., $\langle\Omega\rangle$ (squares) and $\langle_\Omega G\rangle$ (spheres) vs reduced shear rate $\beta_\omega \equiv \tau_\omega\dot{\gamma}$ with relaxation times $\tau_\omega \approx 0.036\dot{\gamma}N^{2.3}$ (precise values are given in the text) which scale with chain length N. Symbols correspond to data for $N = 10$ (open), $N = 20$ (pointed), $N = 30$ (crossed), and $N = 60$ (filled).

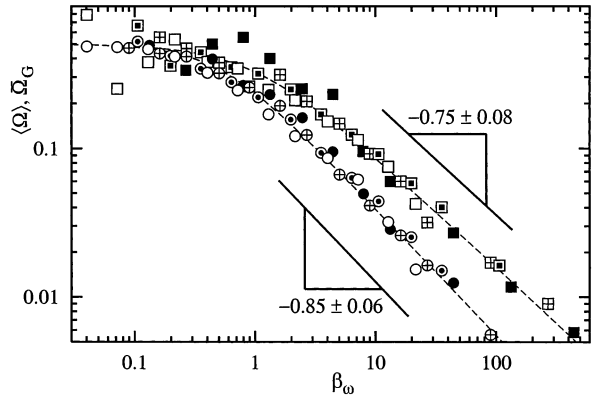

Figure 3. Simulation results for the average angular velocity (squares) $\langle\Omega\rangle$ (eq 9) and the average conformational angular velocity (circles) $\bar{\Omega}_G$ (eq 7) vs reduced shear rate β_ω, cf. Figure 2. Symbols correspond to data for $N = 10$ (open), $N = 20$ (pointed), $N = 30$ (crossed), and $N = 60$ (filled).

confirm that $\langle\omega\rangle \approx \langle\omega_G\rangle$. The inequalities are not surprising, since the corrections due to fluctuations ΔL_z and $\Delta\Theta$ up to second order read

$$\langle\omega\rangle = \left\langle\frac{L_z}{\Theta}\right\rangle \approx \left(1 - \frac{\langle\Delta L_z\Delta\Theta\rangle}{\langle L_z\rangle\langle\Theta\rangle} + \frac{1}{2}\left\langle\left(\frac{\Delta\Theta}{\Theta}\right)^2\right\rangle + ...\right)\bar{\omega} \quad (14)$$

where Θ abbreviates $m(G_{xx} + G_{yy})$; therefore, $\bar{\omega} = \langle L_z\rangle/\langle\Theta\rangle$. We expect $|\langle\omega\rangle| > |\bar{\omega}|$ since ΔL_z and $\Delta\Theta$ are anticorrelated, i.e., $\langle\Delta L_z\Delta\Theta\rangle < 0$. Whenever the polymer unfolds and extends its end-to-end distance, i.e., $\Delta\Theta > 0$, the angular momentum tends to decrease, $\Delta L_z < 0$, due to an increased (common) shape-dependent orientational relaxation time. An analogous relation exists, of course, for the quantities $\langle\omega_G\rangle$ and $\bar{\omega}_G$.

Some qualitative observations concerning the dynamical behavior of the system under study will be presented next, while a more quantitative analysis will be performed in the subsequent section.

III. Dynamics of Rotations and Deformations

A. Qualitative Observations. Flow-induced forces acting on the polymer lead to an orientation dependent deformation, which is schematically depicted in Figure 4, which suggests compression in part a and elongation in part b. According to this picture, disregarding translational motion, such a molecule performs unsteady rotations around its main axis. Periodic rotations are superimposed by a periodic elongation and compression of the main axis. The amount of configurational change during a single rotation depends on the internal viscosity and the elasticity of the molecule and is quantified in section IIIE.

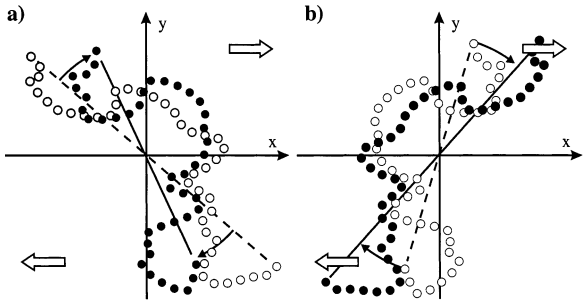

Figure 4. Representative states visualizing the coupling between deformation and orientation of a chain. The qualitative relationship depends on an actual angle χ_G with respect to the flow direction and therefore changes during a full rotation of the chain. Two chain conformations are shown in each part, before (open circles) and after (filled circles) a finite time interval. (a) $-90° < \chi_G < 0°$. The chain is compressed and becomes less anisotropic, whereas in part b, $0° < \chi_G < 90°$, the chain is elongated and its anisotropy is enhanced. Angles are measured counterclockwise.

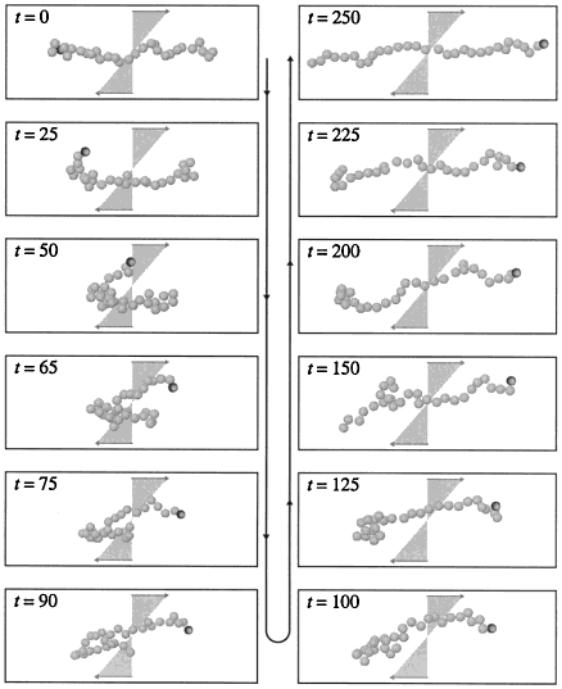

Figure 5. Course of events during a sample rotation of a chain of length $N = 30$ at shear rate $\dot{\gamma} = 0.03$. For each snapshot, the corresponding (dimensionless) time and one of the beads at chain ends is marked to indicate the state of rotation. The reduced angular velocity is 0.45, which is close to the expected value 0.5, and confirmed by Figure 3.

The course of events during a sample rotation of a chain of length $N = 30$ at a small shear rate is shown in Figure 5. At the beginning and at the end of the series of snapshots, the chain is almost perfectly aligned and exhibits strong deformation in the flow plane. Already, during the first third of tumbling period, the end beads change their position with regard to the direction of flow, whereas a time of about $t = 100$ is required to enhance the orientation and deformation of the chain's

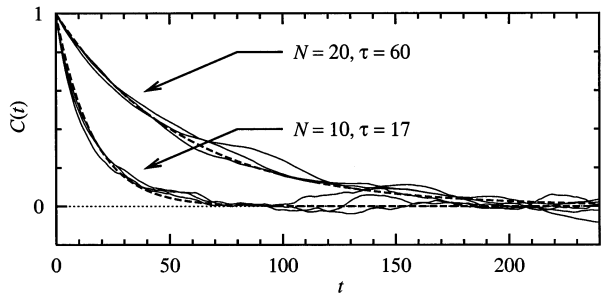

Figure 6. Autocorrelation functions of the squared radius of gyration r_G^2 for two chain lengths and various shear rates in the weak flow regime. In particular, the first set of functions consists of the correlation functions for $N = 10$ at $\dot{\gamma} = 0.0056$, 0.01, and 0.018 (thin solid lines), whereas the second set contains correlation functions for $N = 20$ at $\dot{\gamma} = 0.003$, 0.0056, and 0.01 (thin solid lines). The thick dashed lines denote fit functions of the type $e^{-t/\tau}$, where τ is the correlation time.

conformation. The reduced angular velocity is 0.45, which is close the expected value 0.5, confirmed for small rates by Figure 3. Comparable results were obtained results from Brownian dynamics simulations.[3]

B. Radius of Gyration: Weak Flow Regime. One of the possibilities to extract information from the trajectories returned from MD simulation is to study the stationary autocorrelation function of the squared radius of gyration r_G^2, normalized such that $C(0) = 1$ and $C(\infty) = 0$ for an uncorrelated signal in the long-time limit. Correlation functions have been obtained by both ensemble averaging (varying initial chain conformations) and time averaging (varying reference times) through varying initial conditions.

For the regime of weak flow rates, Figure 6 gives autocorrelation functions for two chain lengths and various small shear rates. The data illustrates, that results are basically independent of the shear rate. In this regime, the configurational correlation time is small compared to the time needed for a full rotation of the chain estimated from the flow rate. In particular, the first set of functions consists of the correlation functions for $N = 10$ at $\dot{\gamma} = 0.0056$, 0.01, and 0.018 (thin solid lines), whereas the second set contains correlation functions for $N = 20$ at $\dot{\gamma} = 0.003$, 0.0056, and 0.01 (thin solid lines). The thick dashed lines denote a exponential decrease of the correlation function with relaxation times $\tau = 17(60)$ for $N = 10(20)$. Because of the selected time frame we do not observe any oscillatory contribution to the autocorrelation function.

For larger shear rates and fixed chain length $N = 10$, a sample is given in Figure 7. chosen to emphasize some general features of $C(t)$ in the range of small and intermediate times. For short times, here $t < 50$, correlations decay quite fast and the slopes are almost independent of the shear rate. This behavior reflects the tendency of the system to "forget" about its initial state (as before for smaller rates). In the range of intermediate times, regular and irregular periodic oscillations occur whose frequencies increase with the strength of the flow parameter. An analogous behavior, while different in nature, is known as director tumbling in liquid crystals, see, e.g., refs 26 and 12 for stiff and partially flexible molecules, respectively. For long flexible molecules the correlation function is strongly affected by the ability of the chain to deform. In particular, the amount of its initial decrease (at short times) should be a signature of the flexibility (or semiflexibility) of the chain.

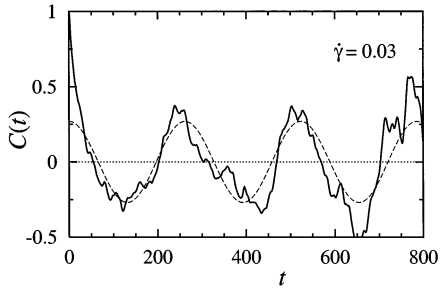

Figure 7. Autocorrelation function for the radius of gyration r_G^2 evaluated for chain length $N = 10$ at shear rate $\dot{\gamma} = 0.03$. A transition takes place from the short-time behavior with a strong decrease to periodic oscillations at intermediate times. The periodicity is illustrated by means of cosine (dashed line) for convenience.

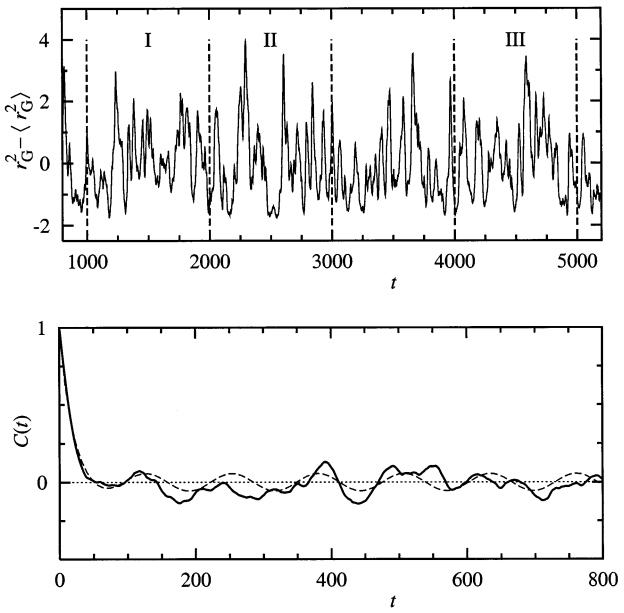

Figure 8. Upper half: deviation of r_G^2 from its long-time average for $N = 10$ and $\dot{\gamma} = 0.1$ plotted vs time. The corresponding correlation function, $C(t)$, evaluated in the time interval $1000 < t < 5000$ (solid line), is shown in the lower half together with a fit to the autocorrelation function introduced in section IIIC (dashed line). Correlations decrease fast and seem to exhibit no significantly oscillatory contribution. A detailed analysis of this time series is performed in Figure 9 for the three intervals, I, II, and III defined in the upper part.

C. Interpretation of the Autocorrelations. The particular findings as well as those for higher shear rates indicate that the autocorrelation function can be superimposed by (i) a monoexponential decay attributed to the initial deformation, with a single relaxation time τ, and (ii) a contribution which is linked with a monoexponential (final) decay of a memory function $M_{final}(t) = \phi \exp(-\Lambda t)$, carrying an amplitude ϕ and an inverse relaxation time Λ. The autocorrelation function is therefore written as a weighted sum

$$C(t) = (1 - b)C_{init}(t; \tau) + bC_{final}(t; \phi, \Lambda) \quad (15)$$

of two contributions C_{init}, C_{final}. On the basis of the memory formalism,[27-29] the time evolution of C is specified by the memory function M, which in turn offers a more convenient interpretation of the underlying microscopic processes. Contribution $C_{init}(t) = \exp(-t/\tau)$ results from a δ-shaped memory function $M_{init}(t) =$

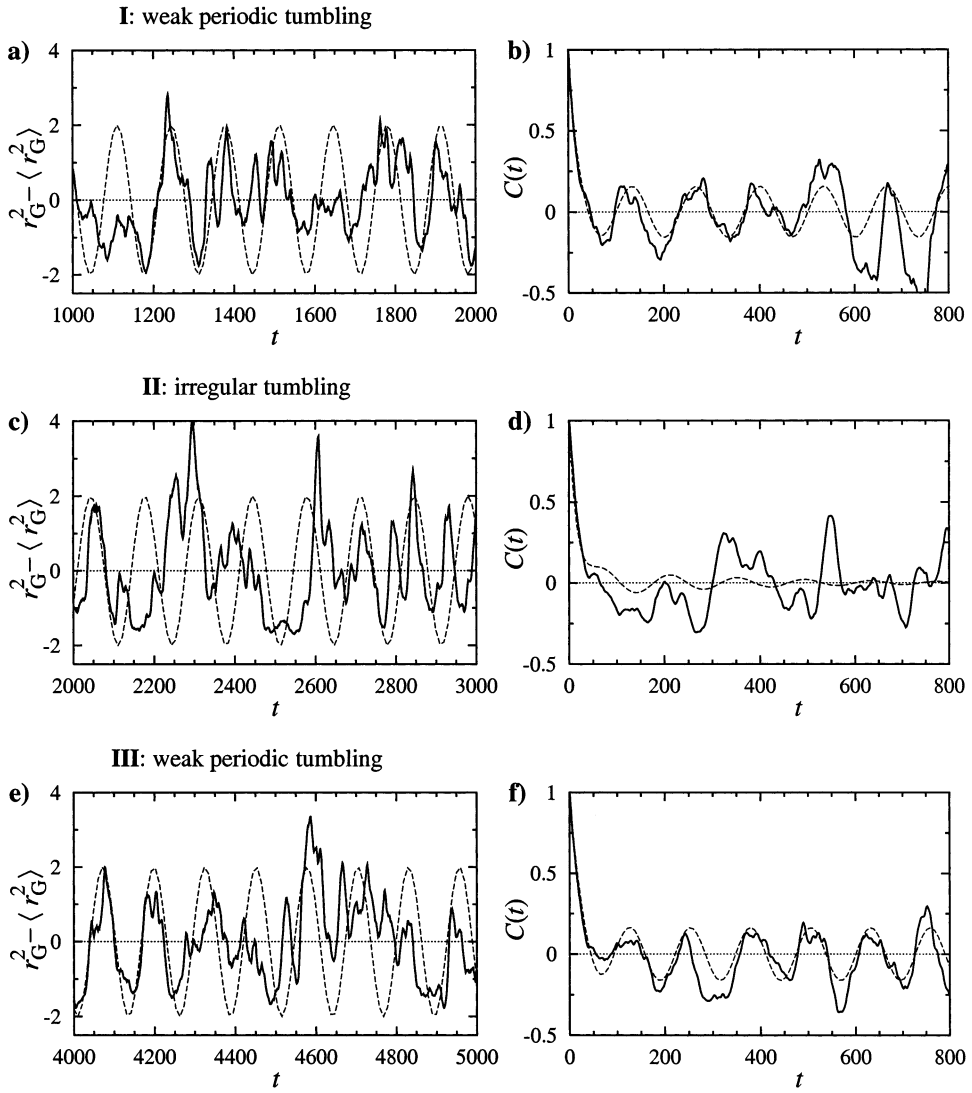

Figure 9. "Local" analysis of the time series depicted in Figure 8 ($r_G^2 - \langle r_G^2 \rangle$ for $N = 10$ and $\dot{\gamma} = 0.1$). Three extracts, I, II, and III, are shown on the left-hand side together with a suitably chosen cosine function in order to emphasize the existence (or the absence) of periodicity. On their right, the corresponding autocorrelation functions and the fit functions (cf. 15) are plotted. A detailed discussion is given in the text.

$\delta(t)/\tau$, while the autocorrelation function, in general, is connected to the memory function by the integro-differential equation

$$\dot{C}(t) = -\int_0^t C(t')M(t - t')\,\mathrm{d}t' \tag{16}$$

which is most conveniently solved for C by a Laplace transformation. With $M_{\mathrm{final}}(t) = \phi \exp(-\Lambda t)$, one has for the transformed quantity $\hat{M}_{\mathrm{final}}(s) = \phi/(s + \Lambda)$, and the Laplace transform of the correlation function C_{final} itself is given by $\hat{C}_{\mathrm{final}}(s) = (s + \Lambda)/(s^2 + \Lambda s + \phi)$. The inverse Laplace transformation yields characteristic solutions depending on whether 4ϕ is larger or smaller than Λ^2. Of relevance in the following is the solution

$$C_{\mathrm{final}}(t) = (\cos 2\omega_{\mathrm{tbl}}t + \Lambda(4\omega_{\mathrm{tbl}})^{-1} \sin 2\omega_{\mathrm{tbl}}t)\mathrm{e}^{-\Lambda t/2} \tag{17}$$

where $\omega_{\mathrm{tbl}}^2 = (\phi - \Lambda^2/4)/4 > 0$ is considered as a squared tumbling frequency. A factor of 2 appears in (17) since the autocorrelation function studied in this section is based on the squared radius of gyration rather than the radius of gyration itself. If the latter case is of interest, ω_{tbl} in (17) should be replaced by $\omega_{\mathrm{tbl}}/2$. Both contributions, C_{init} and C_{final}, are needed to describe the simulation results. The oscillations are themselves damped (via $\Lambda > 0$), the nondamped case ($\Lambda = 0$) corresponds to perfect rotations of the polymer chain. We note that the corresponding power spectrum

$$P(z) \equiv \int_0^\infty C(t) \cos(zt)\,\mathrm{d}t \tag{18}$$

a quantity analyzed in some of the previous works on the rotation of molecules is given within the present ansatz by $P(z) = P_{\mathrm{init}}(z) + P_{\mathrm{final}}(z)$ with $P_{\mathrm{init}}(z) = \tau/[1 + (\tau z)^2]$ and $P_{\mathrm{final}}(z) = \Lambda\phi/[(\phi - z^2)^2 + \Lambda z^2]$. The power spectra given in ref 8, however, are not immediately related to the ones obtained here, since the *yy*-component of the end-to-end distance of a chain rather than its gyration tensor enters their spectra. It should be possible to extract the power spectrum discussed here from experiments of the type presented in.[8] With the help of (1), the power spectrum for the angular momentum is determined by the one for the *yy*-component of the gyration tensor.

D. Radius of Gyration: Intermediate Flow Rate. Data for an intermediate shear rate $\dot{\gamma} = 0.1$, where N

Table 1. Parameters Used to Fit the Data for the Squared Radius of Gyration in the Different Time Zones, Cf. the Upper Part of Figure 8, by the Autocorrelation Function Given in Eq 15[a]

time t	τ	R	b	Λ
1000−5000	17(1)	0.049(5)	0.07(6)	0.003(1)
1000−2000	15(1)	0.047(1)	0.16(1)	$<10^{-4}$
2000−3000	16(2)	0.050(9)	0.05(9)	$<10^{-4}$
4000−5000	18(1)	0.050(1)	0.16(1)	$<10^{-4}$

[a] The parameters b, τ, Λ, and ϕ are defined in section 3.3. Note that ϕ is expressed in terms of $R = (\phi - \Lambda^2/4)^{1/2}$. A number in brackets denotes the uncertainty in the last digit.

$= 10$, is given in Figure 8. The autocorrelation function decreases quite fast and seems to exhibit no significantly oscillatory contribution (although a fit is included in the figure to guide the eyes). The picture changes upon analyzing smaller time intervals. Next we consider the ones marked in the upper part of Figure 8. Inspecting just the time series on the lhs in Figure 9, one observes periodic modulations in the temporal evolution of the radius of gyration during the time intervals I and III, but not so in II. The analysis in terms of the autocorrelation function is provided on the rhs of the same figure. The function $C(t)$ obtained from the simulation is plotted together with the model function (15), whose particular values for b, τ, Λ, and ω_{tbl} are given in Table 1. The distinctive analysis of $C(t)$ reveals weak periodic modulations in the temporal evolution of the radius of gyration during the time intervals I and III, and also in II, reflected by the value obtained for the tumbling frequency ω_{tbl}. The tumbling frequency is almost identical for all these regions. The same is true for the decay time τ, cf. Table 1.

The decay correlation time for the squared radius of gyration characterized by τ depends on the strength of thermal motion due to the surrounding solvent molecules, i.e., on the temperature and the solvent viscosity, as well as on the hydrodynamic effects and geometrical constraints caused by the polymer chain itself. All these effects are taken into account in our NEMD simulation. Values obtained for τ by analyzing the autocorrelation functions of the squared radius of gyration are close to those obtained for the diffusion relaxation time reported in.[10] They are in excellent agreement with the values predicted by the Zimm model, in particular, one has $\tau = 17$, 60, 130, and 450 for $N = 10$, 20, 30, and 60 from simulation, cf. Table 1 for particular values, when $N = 10$. In terms of a power law, this reads $\tau = 0.25N^{3\nu}$ with $\nu = 0.61 \pm 0.01$, whereas the Zimm model predicts $\nu = 0.6$.

The period of the modulation $P = 2\pi\omega_{tbl}^{-1}$ is related to the angular velocity, since it equals half of the tumbling period t_{rot}, and if we refer to Jeffrey's result for the tumbling period P of rigid rods in terms of a tumbling parameter λ, the latter is evaluated via $(1 - \lambda^2)^{1/2} = -2\omega_{tbl}/\dot{\gamma}$. The tumbling frequency ω_{tbl} introduced just below eq 17 provides basically an alternative and independent method to measure the reduced angular velocity $-\Omega_{tbl} = -\omega_{tbl}/\dot{\gamma}$ (or the tumbling parameter) in such intervals of the time series where periodic rotations of the chain are observed. By means of the autocorrelation function of the squared radius of gyration, it is best performed in the range of intermediate flow strengths, since for lower shear rates the conformational changes of the chain during its rotation are very small and in strong flows irregular tumbling tends to dominate.

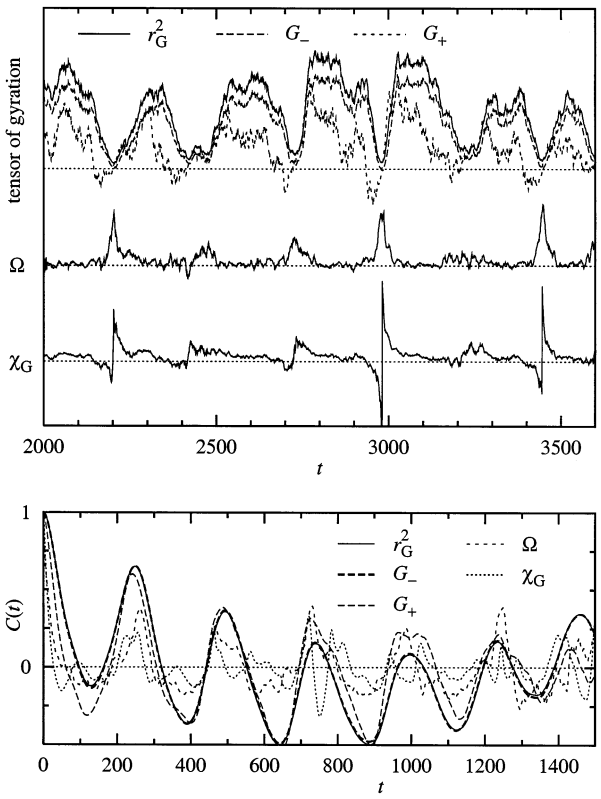

Figure 10. Upper part: temporal evolution of various structural and dynamic quantities plotted in arbitrary units for an extract of a simulation run with $N = 10$ and $\dot{\gamma} = 0.18$. The thin dashed lines mark the null-level of the three sets of curves. Lower part: corresponding autocorrelation functions summarized, which are calculated on the basis of the time interval shown above. For a detailed description of both figures see section IIIE.

E. Angular Velocity and Gyration Tensor: Strong Flow Regime. We now extend these evaluations to other quantities. An example is given in Figure 10 for a simulation run with $N = 10$ at shear rate $\dot{\gamma} = 0.18$. The upper part of the figure shows the time series of the squared radius of gyration r_G^2, two "components" G_+, G_- of the gyration tensor, and the corresponding orientation angle

$$G_+ \equiv G_{xy},\ G_- \equiv (G_{xx} - G_{yy})/2,\quad \tan 2\chi_G \equiv \frac{G_+}{G_-} \qquad (19)$$

and the angular velocity Ω. The bottom part of the figure contains the corresponding autocorrelation functions. The period of modulations seems to be quite insensitive to the choice for a quantity, however, is no one-to-one relationship between fluctuations of an arbitrarily chosen structural quantity and those of the polymer shape. To illustrate this behavior, let us consider the chain orientation angle χ_G and the reduced angular velocity Ω for a rectangular arrangement of a chain made of four beads in the shear plane with edges of length b_x, b_y parallel to x- and y-axes of the coordinate system. The chains tensor of gyration is then completely specified by the diagonal elements $G_{xx} = b_x^2$ and $G_{yy} = b_y^2$, since the other components vanish identically. According to eq 19, χ_G becomes either 0 or 90°, depending on the sign of $2G_- = b_x^2 - b_y^2$. Therefore, small conformational changes around $b_x^2 = b_y^2$ might lead to discontinuous jumps of the chain orientation angle and give rise to the rapid decrease of correlations observed

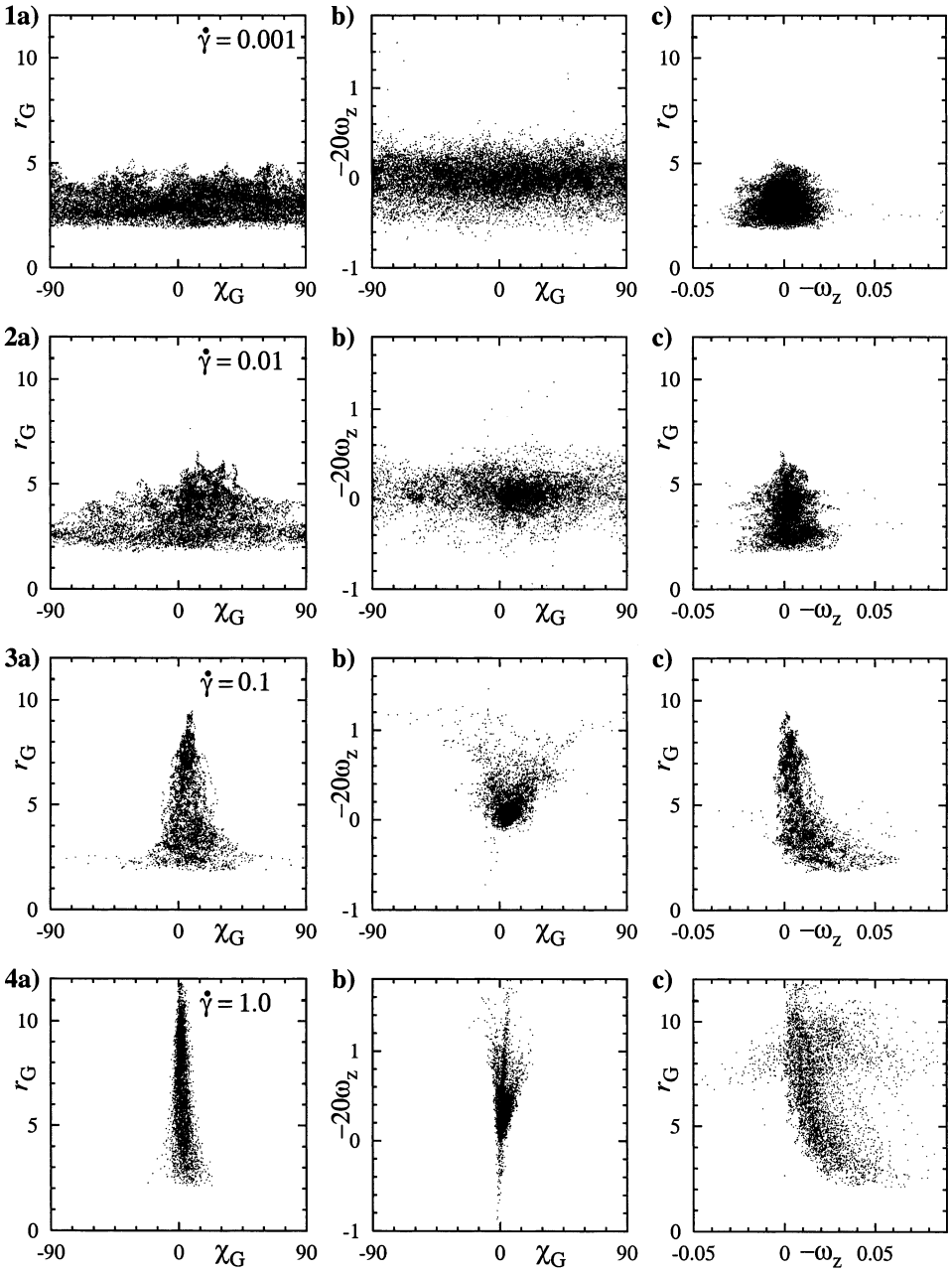

Figure 11. Cross-correlations of the radius of gyration r_G, the chain orientation angle χ_G, and the angular velocity ω_z as obtained for $N = 30$ at shear rates (1) $\dot{\gamma} = 0.001$, (2) $\dot{\gamma} = 0.01$, (3) $\dot{\gamma} = 0.1$, and (4) $\dot{\gamma} = 1.0$. Each of the three columns is devoted to a different combination of three quantities: i.e., column a, r_G vs χ_G; column b, ω_z vs χ_G; and column c, r_G vs ω_z. Typically, the plots contain 10 000−30 000 points of data subsequently evaluated every 200 integration steps. A detailed discussion is given in the text.

in Figure 10. Although its origin is different, a similar behavior is found for the correlation function of the angular velocity. Here, the strong effect of short time fluctuations stems from the thermal contribution of the particle velocities.

The strength of short time fluctuations is only partly visible in Figure 10, since the time series is smoothed for the present purpose by a weak averaging convolutional low pass filter.[30] Accordingly, the main purpose of this figure is to show the systematic time evolution for various quantities over long times and to emphasize their interrelations. Each time interval bounded by adjacent major minima of the squared radius of gyration, consists of the same sequence of events. At beginning of such a period, G_- is slightly negative and G_+ is zero, which corresponds to an orientation angle of 90°. Then both "components" G_+ and G_- as well as the radius of gyration rapidly increase while the chain successively starts to align along the x-axis. However, before r_G^2 and G_- reach their maximum values, both dominated by the xx-component of tensor of gyration, its nondiagonal component $G_{xy} = G_+$ begins to decrease. In the following, the chain slowly approaches an orientation along the flow direction. At this time, the deformation already starts to decrease, since the efficiency by which the velocity field affects the polymer beads is already drastically reduced. In the final period, the "component" G_+ and the orientation angle take negative values for a comparatively short period, which changes when G_+ increases again, becomes zero and the next major minimum of the radius of gyration is reached. A similar course of events is shown in Figure 5 by means of a

sample series of snapshots. Notice that the remaining *zz*-component of the gyration tensor does not vanish, but decreases with increasing shear rate. The decrease, however, is less pronounced than the increase of the G_--component.

F. Cross-Correlations. Some of the described processes pass faster than others, depending on the reduced angular velocity. In particular, in Figure 10, the width of minima of r_G^2 are the smaller the more the angular velocity exceeds its mean value (comparative minima at $t \approx 2200$, 3000, and 3400 and correlate with values at $t \approx 2800$ and 3200). On the other hand, times where the actual radius of gyration takes large values coincide with times where the actual angular velocity ω vanishes. Cross-correlations between different measures needed to interpret these findings are resolved in Figure 11 for $N = 30$. The data illustrates an increasing synchronization of a number of quantities (to be specified below) with increasing shear rate. The plots are organized in a 3×4 table of figures consisting of three columns, each devoted to a pair of quantities at four different shear rates, (1) $\dot\gamma = 0.001$, (2) $\dot\gamma = 0.01$, (3) $\dot\gamma = 0.1$, and (4) $\dot\gamma = 1.0$. In column a, the radius of gyration is plotted vs the chain orientation angle, and no correlation is detectable at low rates. At higher shear rates, the tendency becomes apparent that large values of the radius of gyration go along with orientation angles in the range $0 \le \chi_G \le 2\langle\chi_G\rangle$ and vice versa. This feature is a direct result of the dominating influence of the component G_{xx} on both properties. The graphs in the second column show the interrelation of the angular velocity with the chain orientation angle. Again, there is no correlation detectable close to equilibrium and "rotations in both directions" are almost equal probable. At moderate shear rates, the likelihood of rotations yielding negative angular velocities is slightly enhanced, whereas in the strong flow regime, this direction of rotation is the dominating one. Only in the strong flow regime is the probability of high values for Ω somewhat larger for the less oriented conformations than for those with $\chi_G \approx \langle\chi_G\rangle$. In the third column, c, the radius of gyration is plotted vs the angular velocity, a signal which turns out to be rather uncorrelated at small and intermediate shear rates. At higher flow strengths, high values of the angular velocity are likely to go along with small values of the radius of gyration, whereas elongated chains tend to rotate rather slowly. Remarkably, this tendency partially vanishes at even higher shear rates, indicating the absence of periodic rotations and a transition to an irregular or chaotic rotational behavior.

IV. Conclusions

In this article we established the validity of the "angular momentum−optic rule" in its two representations, eqs 1 and 7, for a dilute polymer solution in the case of a steady shear flow by means of NEMD computer simulation. The microscopic model for a polymer molecule immersed in a solution composed of monomers incorporates the effects of hydrodynamic interaction through the presence of explicit solvent monomers, and of finite stretchability of chains. The complex dynamics observed here is inherently connected with the nonlinearities in the equations of motion which come along with finite extendability of polymer chains. Significant stretching of bonds, i.e., departures from linear elastic forces, are present above reduced shear rates $\beta \approx 5$. These, however, do not immediately produce departures from the "angular momentum−optic rule" at high rates since central forces between monomers are used. The microscopic dynamics underlying the simple rule and, in particular, times series, the correlated rotation and deformation behavior, and cross-correlations between several structural quantities have been investigated in detail. These results should allow to improve more efficient implementations[4] which aim to describe polymer dynamics considering hydrodynamic interactions by using ad hoc Langevin equations (with a certain colored noise) for the conformational variables.[31,5]

Acknowledgment. This work has been conducted under the auspices of the Sonderforschungsbereich SFB 448 "Mesoskopisch strukturierte Verbundsysteme" of the Deutsche Forschungsgemeinschaft (DFG). Financial support is gratefully acknowledged. Part of this work was done while S.H. and M.K. stayed at the Institute for Theoretical Physics, Santa Barbara, CA, with support in part by the National Science Foundation under Grant No. PHY99-07949.

References and Notes

(1) Rouse, P. *J. Chem. Phys.* **1953**, *21*, 1272. Zimm, B. *J. Chem. Phys.* **1956**, *24*, 269. Peterlin, A.; Heller, W.; Nakagaki, M. *J. Chem. Phys.* **1958**, *28*, 470. Warner, H. *Ind. Eng. Chem. Fundam.* **1972**, *11*, 379. de Gennes, P. G. *J. Chem. Phys.* **1974**, *60*, 5030. Hinch, E. *J. Fluid Mech.* **1976**, *75*, 765. Magda, J.; Larson, R.; Mackay, M. *J. Chem. Phys.* **1988**, *89*, 2504. Wedgewood, L.; Öttinger, H.; *J. Non-Newtonian Fluid Mech.* **1988**, *27*, 245. Wedgewood, L.; Ostrov, D.; Bird, R. B. *Fluid Mech.* **1991**, *40*, 119.

(2) Fuller, G. G.; Leal, L. G. *Rheol. Acta* **1980**, *19*, 580.

(3) Liu, T. W. *J. Chem. Phys.* **1989**, *90*, 5826. Doyle, P. S.; Shaqfeh, E. S. G.; Gast, A. P. *J. Fluid. Mech.* **1997**, *334*, 251. Bossart, J.; Öttinger, H. C. *Macromolecules* **1997**, *30*, 5527. Lyulin, A. V.; Adolf, D. B.; Davies, G. R. *J. Chem. Phys.* **1999**, *111*, 758.

(4) Jendrejack, R. M.; Graham, M. D.; de Pablo, J. J. *J. Chem. Phys.* **2000**, *113*, 2894. Kröger, M.; Alba-Pérez, A.; Laso, M.; Öttinger, H. C. *J. Chem. Phys.* **2000**, *113*, 4767.

(5) Suen, J. K. C.; Joo, Y. L.; Armstrong, R. C. *Annu. Rev. Fluid Mech.* **2002**, *34*, 417.

(6) Link, A.; Springer, J. *Macromolecules* **1993**, *26*, 464. Lee, E. C.; Solomon, M. J.; Muller, S. J. *Macromolecules* **1997**, *30*, 7313.

(7) Cerf, R. *J. Chim. Phys.* **1969**, *68*, 479. Bazua, E. R.; Williams, M. C. *J. Polym. Sci.* **1974**, *12*, 825.

(8) Smith, D. E.; Babcock, H. P.; Chu, S. *Science* **1999**, *283*, 1724.

(9) Pierleoni, C.; Ryckaert, J.-P. *Phys. Rev. Lett.* **1991**, *61*, 2992; *Chem. Phys.* **1992**, *96*, 8539; *Macromolecules* **1995**, *28*, 5097. Hess, S.; Aust, C.; Kröger, M. *Cah. Rheol. (Fr.)* **1996**, *15*, 1.

(10) Aust, C.; Kröger, M.; Hess, S. *Macromolecules* **1999**, *32*, 5660.

(11) de Gennes, P. G. *J. Chem. Phys.* **1974**, *60*, 5030.

(12) Chaubal, C. V.; Leal, L. G. *J. Polym. Sci. B* **1999**, *37*, 281. *J. Non-Newtonian Fluid Mech.*, in press.

(13) Szeri, A. J. *J. Rheol.* **1995**, *39*, 873.

(14) Rienäcker, G.; Kröger, M.; Hess, S. Chaotic and regular shear-induced orientational dynamics of nematic liquid crystals. *Physica A* **2002**, in press.

(15) Chillingworth, D. R. J.; Alonso, E. V.; Wheeler, A. A. *J. Phys. A: Math. Gen.* **2001**, *34*, 1393.

(16) Debye, P. *J. Chem. Phys.* **1946**, *14*, 636.

(17) Ceperly, D.; Kalos, M.-H.; Lebowitz, J. L. *Phys. Rev. Lett.* **1978** , *41*, 313; *Macromolecules* **1981**, *14*, 1472. Kremer, K.; Grest, G. S. *J. Chem. Phys.* **1990**, *92*, 5057; Dünweg, B.; Kremer, K. *Phys. Rev. Lett.* **1991**, *61*, 2996; *J. Chem. Phys.* **1993**, *99*, 6983.

(18) Kröger, M.; Loose, W.; Hess, S. *J. Rheol.* **1993**, *37*, 1057.

(19) Larson, R. G. *Constitutive Equations for Polymer Melts and Solutions*; Butterworths: Boston, MA, 1988.

(20) Weeks, J. D.; Chandler, D.; Andersen, H. C. *J. Chem. Phys.* **1971**, *54*, 5237.

(21) Hess, S.; Kröger, M.; Voigt, H. *Physica A* **1998**, *250*, 58.
(22) Warner, H. R. *Ind. Eng. Chem. Fundam.* **1972**, *11*, 379.
(23) Hoover, W. G. *Molecular Dynamics*; Lecture Notes in Physics 258, Springer: New York, 1986.
(24) Lees, A. W.; Edwards, S. F. *J. Phys. C* **1972**, *5*, 1921.
(25) Yasuda, K.; Armstrong, R. C.; Cohen, R. E. *Rheol. Acta* **1981**, *20*, 163.
(26) Jeffrey, G. B. *Proc. R. Soc. London Ser. A* **1922**, *102*, 171.
(27) Hansen, J. P.; McDonald, I. R. *Theory of Simple Liquids*; Academic Press: London, 1986.
(28) McQuarrie, D. A. *Statistical Mechanics*; Harper & Row: New York, 1976.
(29) Evans, D. J.; Morriss, G. P. *Statistical Mechanis of Nonequilibrium Liquids*; Academic Press: London, 1990.
(30) Bock, R. D.; Krischer, W. *The Data Analysis BriefBook*; Springer: Berlin, 1998.
(31) Öttinger, H. C. *Stochastic processes in polymeric fluids*; Springer: Berlin, 1996.

MA020710K